Supplement of

New experiments to probe the role of fractures in bedrock on river erosion rate and processes

Marion Fournereau[1], Laure Guerit[1], Philippe Steer[1], Jean-Jacques Kermarrec[1], Paul Leroy[2], Christophe Lanos[3], Hélène Hivert[4], Claire Astrié[1], Dimitri Lague[1]

[1]Univ Rennes, CNRS, Géosciences Rennes, UMR 6118, 35000, Rennes, France
[2]Univ Rennes, CNRS, Lidar Platform, OSERen, UAR3343, Rennes, France
[3]Univ Rennes, Laboratoire de Génie Civil et Génie Mécanique, Rennes, France
[4]UnivRennes, Inria, Géosciences Rennes - UMR 6118, IRMAR - UMR 6625, F-35000 Rennes, France

Correspondence to: Marion Fournereau (marion.fournereau@univ-rennes.fr) and Laure Guerit (laure.guerit@univ-rennes.fr)

Supplement S1 – Impact of the quantity of water added to the concrete mix on its compacity

To evaluate the impact of water content on concrete paste compacity, we prepare four concrete mixes with varying water content with respect to the reference mix (-20%, -10%, +10%, and +20%) while maintaining a constant cement-to-sand ratio. Figure S1 illustrates the ratio of the air (v_a) and water (v_w) volumes with respect to the total volume according to the content of water. We also show the resulting compacity for each mix. An increase in water content leads to a rise in v_w, while the entrapped air volume ratio (v_a) decreases due to increased viscosity, and conversely. The reduction in air volume compensates for the increase in water, keeping the overall paste compacity relatively stable.

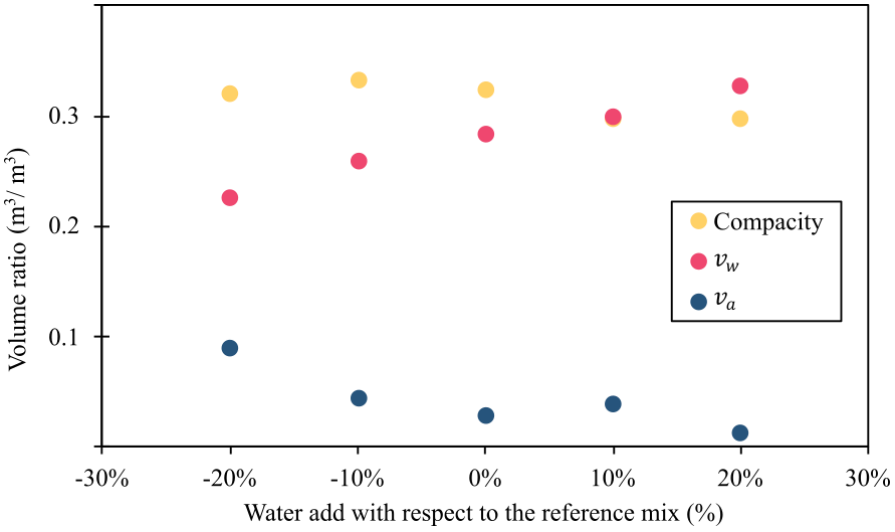

Figure S1: Comparison between air (v_a) and water (v_w) volume ratio, together with compacity of the concrete paste according to the water content.

Supplement S2 – Comparison between topographic and mass loss estimations of cumulative erosion and erosion rate

Our study analyses the erosion of our experimental substrates from 3D topographic evolution. However, it is more common to use the total mass loss (Sklar and Dietrich, 2001; Turowski et al., 2023).

To make sure that our 3D method is accurate, and to be consistent with the literature, we weighed the column every 2 minutes in addition to recording the topography via photogrammetry (see main text, Experimental protocol). Here, we compare the erosion rate obtained by mass loss through time with the erosion rate obtained by topographic loss through time (Fig. S2). Erosion rates obtained by these two methods follow the same dynamics both in cumulative erosion (in mm and in g) and in erosion rate over time (in mm/min and g/min) (Fig. S2). In some cases (e.g., Fig. S2-1), we observe some limited deviations and we suggest that it is related to variations in the remaining amount of water in the column when we weighted it. In a few experiments, we observe more intense deviation especially in the cumulated erosion (Fig. S2-10) that we are not able to explain with our data. Yet, we note that the erosion rates follow similar dynamics (Fig. S2-10). As this study is mainly based on erosion rates (and not on cumulative erosion), we only use the topographic data to characterize erosion dynamics.

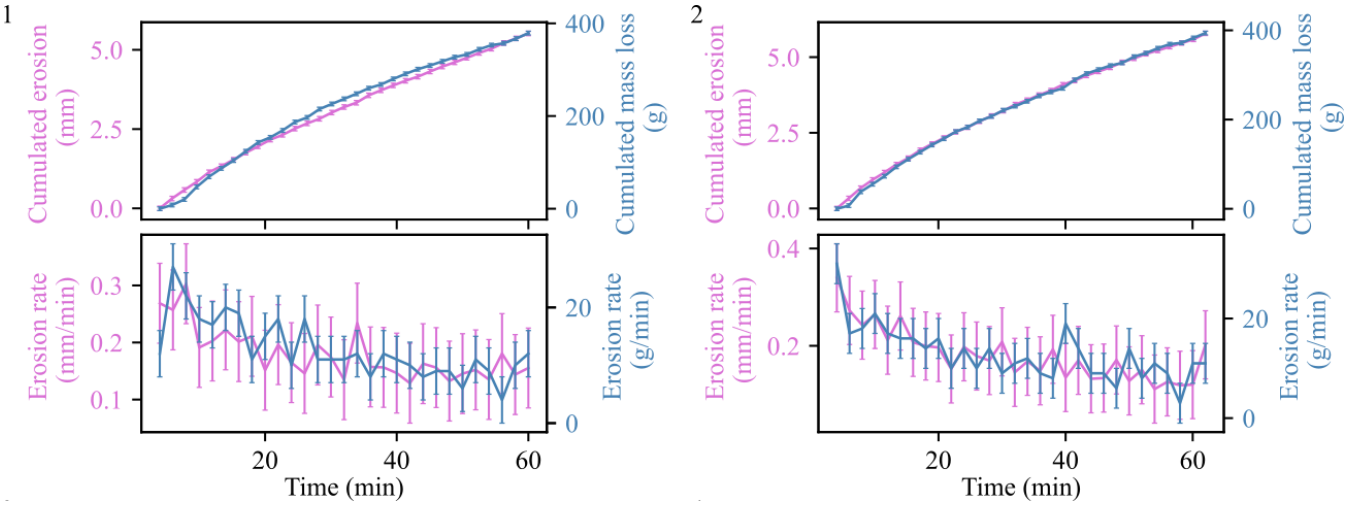

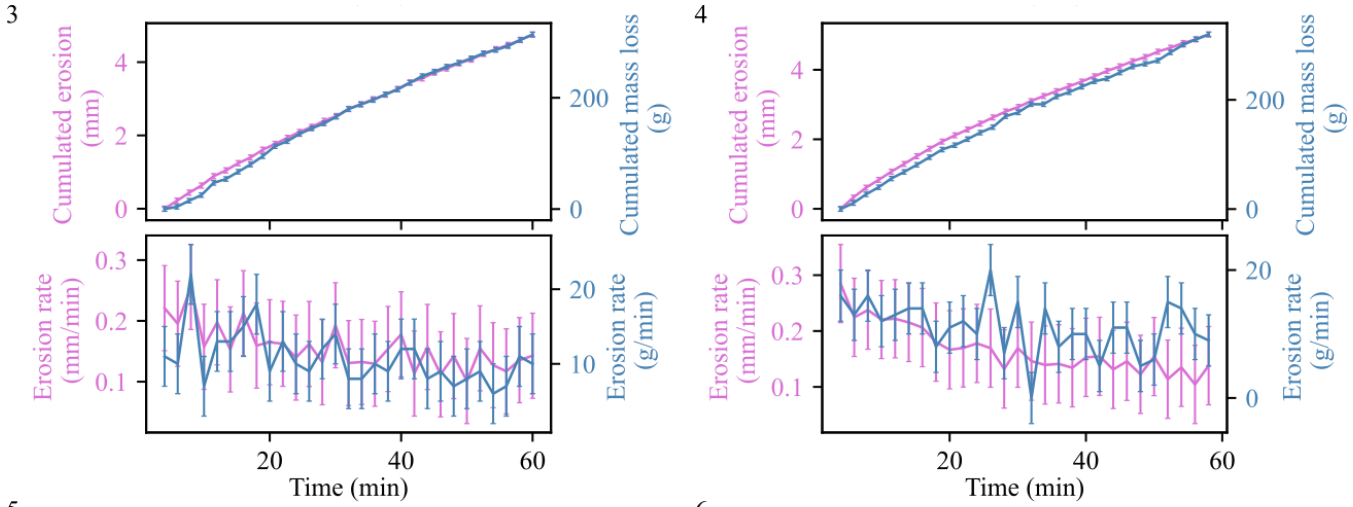
3
Cumulated erosion (mm)
Cumulated mass loss (g)
Erosion rate (mm/min)
Erosion rate (g/min)
Time (min)

4
Cumulated erosion (mm)
Cumulated mass loss (g)
Erosion rate (mm/min)
Erosion rate (g/min)
Time (min)

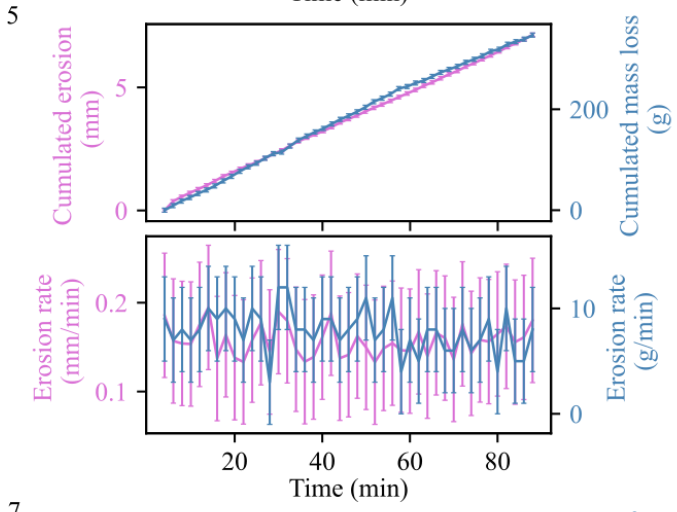
5
Cumulated erosion (mm)
Cumulated mass loss (g)
Erosion rate (mm/min)
Erosion rate (g/min)
Time (min)

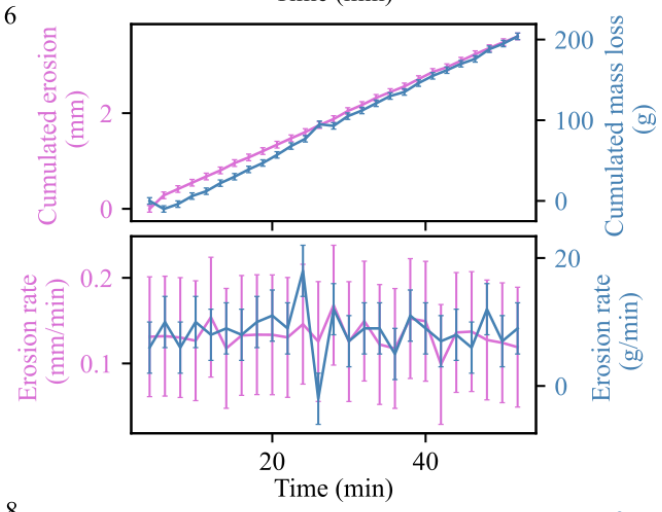
6
Cumulated erosion (mm)
Cumulated mass loss (g)
Erosion rate (mm/min)
Erosion rate (g/min)
Time (min)

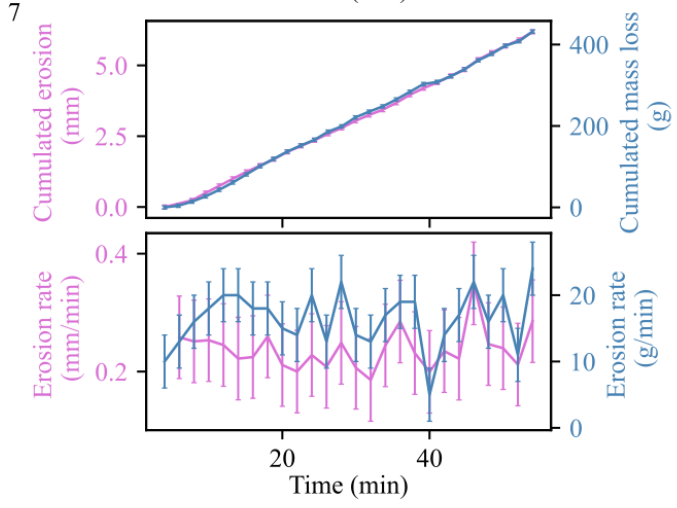
7
Cumulated erosion (mm)
Cumulated mass loss (g)
Erosion rate (mm/min)
Erosion rate (g/min)
Time (min)

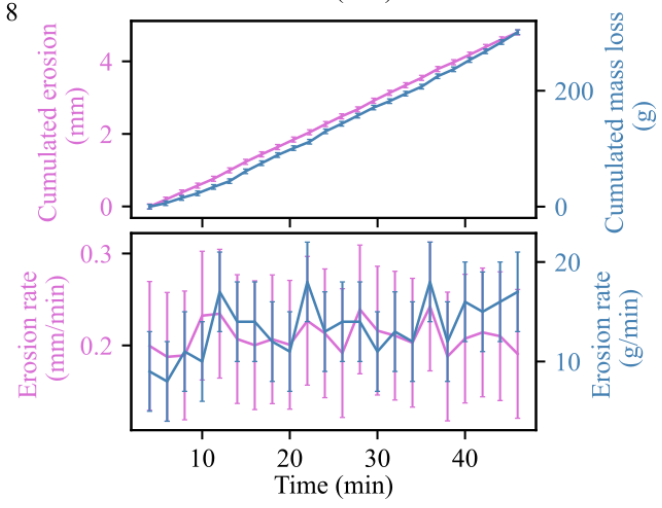
8
Cumulated erosion (mm)
Cumulated mass loss (g)
Erosion rate (mm/min)
Erosion rate (g/min)
Time (min)

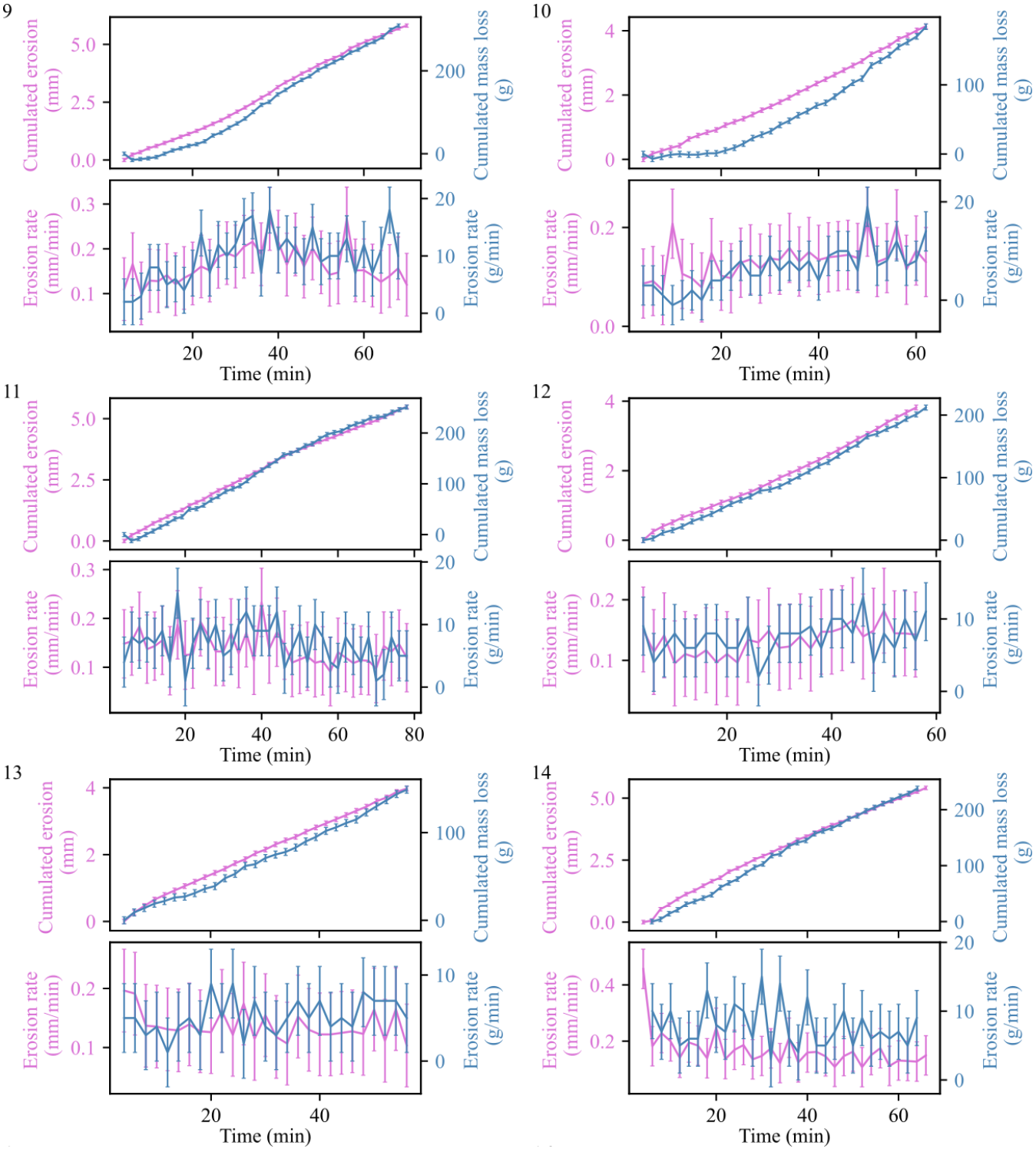
9
Cumulated erosion (mm)
Cumulated mass loss (g)
Erosion rate (mm/min)
Erosion rate (g/min)
Time (min)
10
Cumulated erosion (mm)
Cumulated mass loss (g)
Erosion rate (mm/min)
Erosion rate (g/min)
Time (min)
11
Cumulated erosion (mm)
Cumulated mass loss (g)
Erosion rate (mm/min)
Erosion rate (g/min)
Time (min)
12
Cumulated erosion (mm)
Cumulated mass loss (g)
Erosion rate (mm/min)
Erosion rate (g/min)
Time (min)
13
Cumulated erosion (mm)
Cumulated mass loss (g)
Erosion rate (mm/min)
Erosion rate (g/min)
Time (min)
14
Cumulated erosion (mm)
Cumulated mass loss (g)
Erosion rate (mm/min)
Erosion rate (g/min)
Time (min)

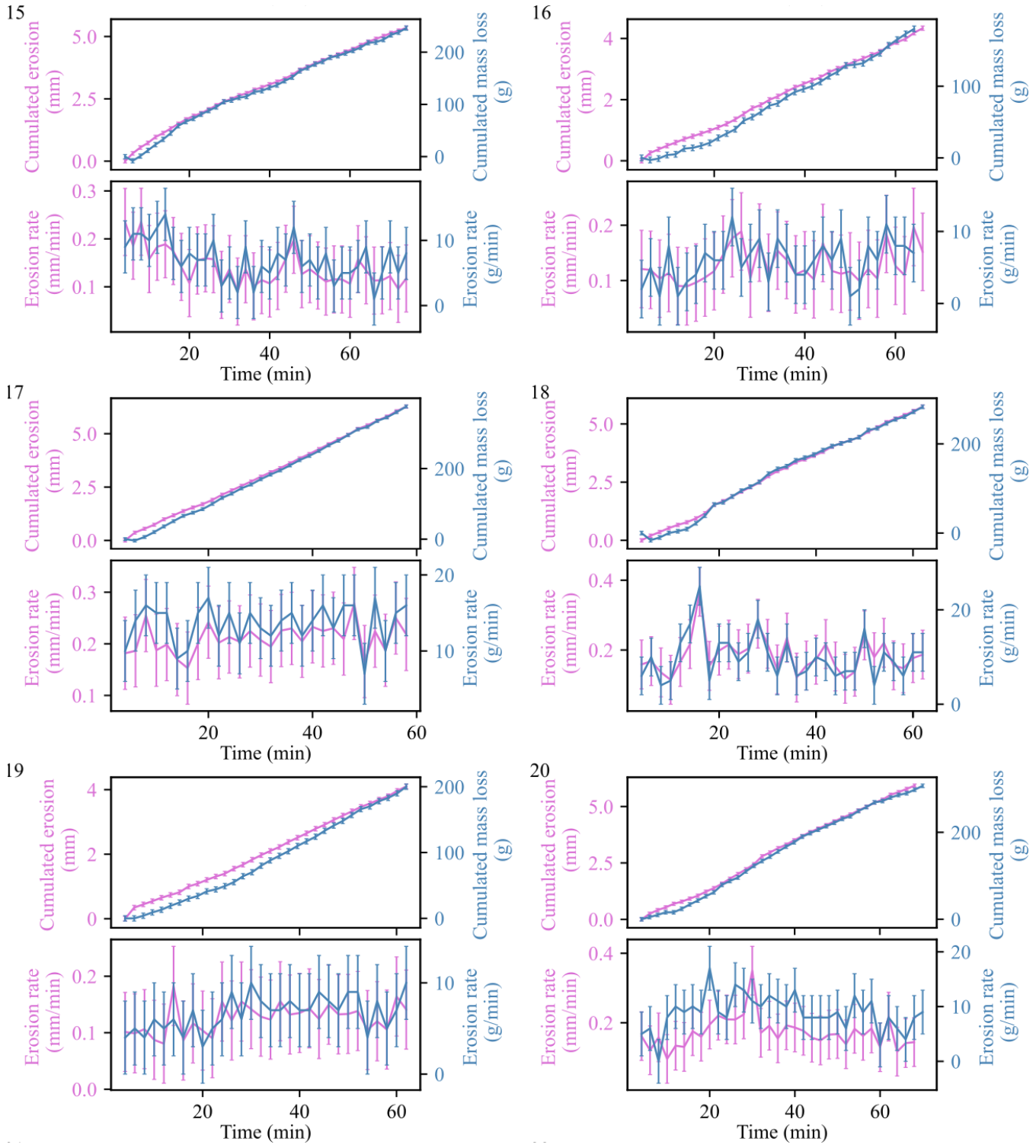
15
16
17
18
19
20
Cumulated erosion (mm)
Cumulated mass loss (g)
Erosion rate (mm/min)
Erosion rate (g/min)
Time (min)

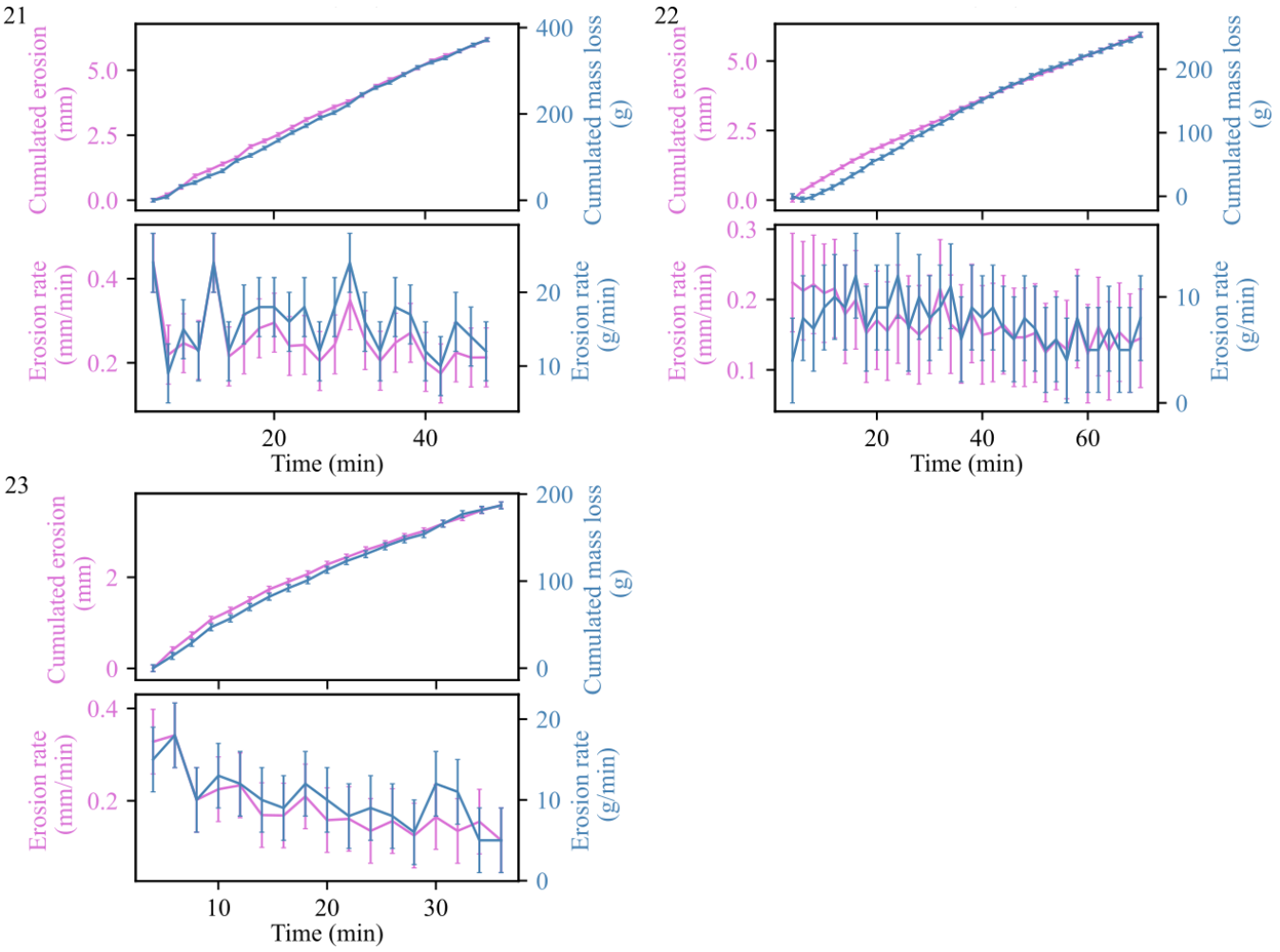

Figure S2: Comparison of cumulative erosion (top) and erosion rate (bottom) derived from topographic evolution (pink) and mass loss (blue) through time, for the experiments used in this study. Panel numbers refer to the experiment number in Table 1 (main text).

Supplement S3: Geometry of concrete fragments retrieved during the emptying phase

When plucking occurs during the experiment, we sometimes find some concrete fragments mixed with the granite grains when we empty the column before to weight it (see main text, Section 2.2). For 8 experiments, we measured with a calliper the 3 axis (a-, b-, c-axis, corresponding to the large, intermediate and small axis) of the fragments to characterize their geometry and look for a relationship with the fracture network geometry (Fig. S3). For practical reasons (i.e., the minimum size that can be accurately measured by hand), we focus on fragments with a b-axis of minimum 5 mm. We note that the fragments may have been eroded after their removal from the disk so that their measured sizes might not correspond to their initial ones. In addition, we found a lot of smaller fragments that could be either small chunks removed from the disk itself or from the larger

fragments. We first compare the a- and b- axis of the fragments (i.e, we look at them in map view). We observe that the b-axis is most of the time smaller than the a-axis, implying that most fragments have a rectangular shape even when they come from a square fracture network (Fig. S3a). For example, the experiments with a fracture density of 100 m^{-1} correspond to the 20/20 mm network. Even when the network is rectangular, the geometry might not be kept as for example, the experiment with a density of 145 m^{-1} corresponds to fragments coming from a rectangular-shaped fracture network (10/20 mm) and some fragments are only a portion of it (10 by 10 mm).

Then, we look at the relationship between the area of the fragments (defined as the a-axis times the b-axis) to the c-axis. Results are quite scattered (Fig. S3b) and it seems that two groups emerge according to the fracture density (purple/pink vs blue dots). In both cases, it seems that large fragments are associated with larger c-axis. This is in line with the results shown in Fig. 7 in the main text, based on the geometry of plucked blocks.

Keeping in mind the limitations mentioned above, these results support the idea that the larger the plucked area, the deeper the block as it is not possible to remove a very thin block by plucking.

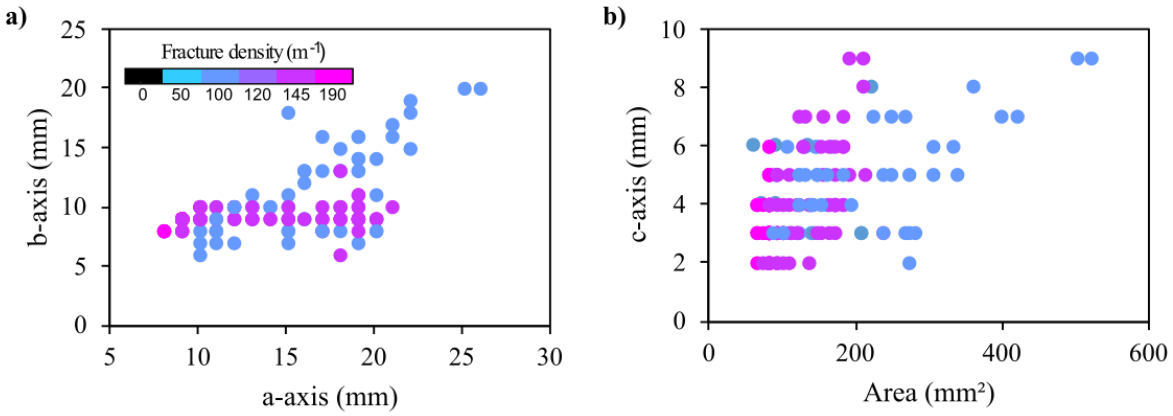

Figure S3: Geometry of the fragments retrieved during some experiments with a) the a-axis with respect to the b-axis, and b) the c-axis with respect to the fragment's area (defined as a-axis × b-axis) (data used in this graph are from experiments numbered 7, 11, 13, 14, 17, 18, 21 and 23 in Table 1).

Supplement S4: Variability of total erosion radial profiles

To better understand the spatial profile of erosion, we extract the radial profile of total erosion after 40 min of run, for each experiment and we group the experiments according to their total erosion by plucking (see main text, Fig. 8 and Table 1). For each experiment, we also observe a large spread especially as we go further from the centre of the disk and this scatter increases with the contribution of plucking (Fig. S4). For example, at 70 mm from the centre, values range between 6 and 12 mm when there is no plucking and between 2 and 18 mm when there is more than 10 % plucking.

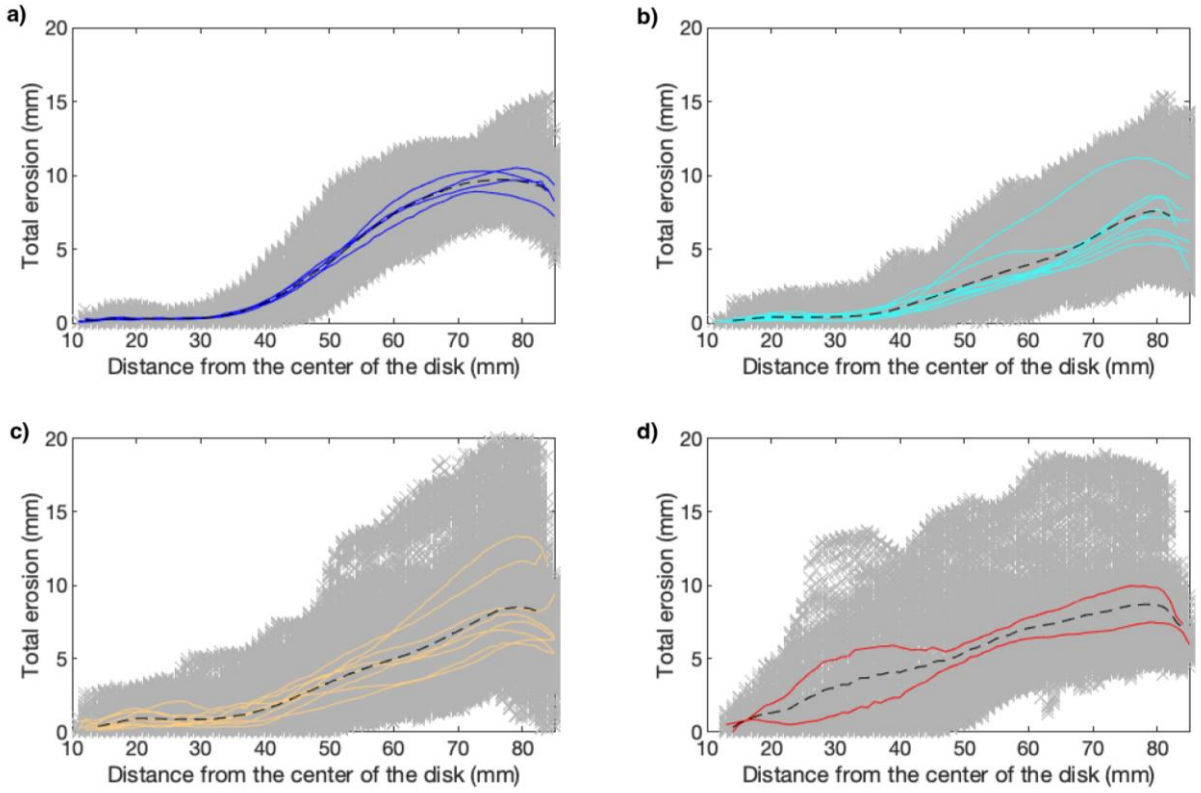

Figure S4: Total erosion after 40 min of run according to the distance from the centre of the disk, for experiments grouped after their total erosion by plucking with a) 0 %, b) less than 5 % c) from 5 to 10 % and d) more than 10 % of erosion by plucking. Grey crosses are for all the measured values, the coloured lines are the average profiles of the experiments and the dotted lines are the average of each group.

References

Sklar, L. and Dietrich, W.: Sediment and rock strength control on river incision into bedrock, Geology, 29, 1087–1090, https://doi.org/10.1130/0091-7613(2001)029<1087:SARSCO>2.0.CO;2, 2001.

Turowski, J. M., Pruß, G., Voigtländer, A., Ludwig, A., Landgraf, A., Kober, F., and Bonnelye, A.: Geotechnical controls on erodibility in fluvial impact erosion, Earth Surface Dynamics, 11, 979–994, https://doi.org/10.5194/esurf-11-979-2023, 2023.